Control of Chirality, Bond flexing and Anharmonicity in an Electric Field

Zi Li, Xing Nie[1], Tianlv Xu[1], Shuman Li[1], Yong Yang[1], Herbert Früchtl[2], Tanja van Mourik[2], Steven R. Kirk[*1], Martin J. Paterson[3], Yasuteru Shigeta[4] and Samantha Jenkins[*1]

[1]*Key Laboratory of Chemical Biology and Traditional Chinese Medicine Research and Key Laboratory of Resource National and Local Joint Engineering Laboratory for New Petro-chemical Materials and Fine Utilization of Resources, College of Chemistry and Chemical Engineering, Hunan Normal University, Changsha, Hunan 410081, China*

[2]*EaStCHEM School of Chemistry, University of Saint Andrews, North Haugh, St Andrews, Fife KY16 9ST, Scotland, United Kingdom.*

[3]*Institute of Chemical Sciences, School of Engineering and Physical Sciences, Heriot-Watt University, Edinburgh, EH14 4AS, UK*

[4]*Center for Computational Sciences, University of Tsukuba, Tsukuba 305-8577, Japan*

email: steven.kirk@cantab.net
email: samanthajsuman@gmail.com

We located 'hidden' S-character chirality in formally achiral glycine using a vector-based interpretation of the total electronic charge density distribution. We induced the formation of stereoisomers in glycine by the application of an electric field. Control of chirality was indicated from the proportionate response to a non-structurally distorting electric field. The bond-flexing was determined to be a measure of bond strain, which could be a factor of three lower or higher, depending on the direction of the electric field, than in the absence of the electric field. The bond-anharmonicity was found to be approximately independent of the electric field. We also compared the formally achiral glycine with the chiral molecules alanine and lactic acid, quantifying the preferences for the S and R stereoisomers. The proportional response of the chiral discrimination to the magnitude and direction of the applied electric field indicated use of the chirality discrimination as a molecular similarity measure.

1. Introduction

The existence of chirality has important implications[1]–[3] and the origin of chiral asymmetry[4] in molecular biology is one of the great mysteries in the understanding of the origin of life[5]–[12]. In 1848 Louis Pasteur proposed biomolecular homochirality as a possible simple 'chemical signature of life'[13].

A recent publication by Francl expressed skepticism about using binary measures for chirality and instead proposed considering continuous measures of chirality[14]. In particular the discussion focused around continuous (non-binary) chirality, as developed by Zahrt and Denmark, who argued that chirality is a transmissible property.[15] They used the method of Zabrodsky and Avnir[16] to determine the degree of chirality, based on computing the minimal distance that the vertices of a shape must be moved to attain an achiral system. Zahrt and Denmark argue that the degree of chirality of molecules depends on their ability to transmit that information to another molecule and to differentiate enantiomers. Mislow, Bickart and others presented the idea that a molecule is a vector of measurable properties, such as optical activity, and therefore chirality is not a binary property, but a continuous quantity[14], [16], [17]. A multidisciplinary review by Petitjean on the relationship between the degree of chirality and symmetry involved discussion of concepts such as similarity, disorder and entropy[18]. Jamróz *et al.* proposed a continuous measure of chirality based on topology, creating the concept of Property Space and similarity between enantiomers for use as a quantitative structure activity relationship (QSAR) measure[19]. Molecular similarity measures[20]–[24] have found frequent use in QSAR investigations, some explicitly including considerations of conventional chirality[25]–[29].

Conventional (scalar) QTAIM is insufficient to distinguish S and R stereoisomers at the energy minimum and can at best quantify the asymmetry of the charge density distribution in the form of the bond critical point ellipticity ε. Next generation QTAIM (NG-QTAIM)[30], a vector-based quantum mechanical theory constructed within the quantum theory of atoms in molecules (QTAIM)[31] using the stress tensor, can differentiate the S and R stereoisomers for all values of the torsion θ, $-180.0° \leq θ \leq +180.0°$. In this investigation we use Bader's formulation of the stress tensor[32] and NG-QTAIM on the basis of the superior performance of the stress tensor compared with vector-based QTAIM for distinguishing the S and R stereoisomers of lactic acid[33]. The most (facile) preferred direction of electron charge density accumulation determines the direction of bond motion[34]. Within the electron-preceding perspective a change in the electronic charge density distribution that defines a chemical bond results in a change in atomic positions[35]. Bone and Bader later proposed that the direction of motion of the atoms that results from a slightly perturbed structure coincides with the direction of motion of the electrons[36]; this was subsequently confirmed[37], [38].

In this investigation we will seek to locate the presence of chiral character for electron density and manipulate induced chirality in glycine by varying the direction and magnitude of an applied electric (**E**)-field to create S and R stereoisomers. The application of an **E**-field will induce symmetry-breaking

changes to the length of the C-H bonds attached to the alpha carbon atom (C1) of formally achiral glycine, as previously studied by Wolk *et al.* in achiral glycine[39], see **Scheme 1**.
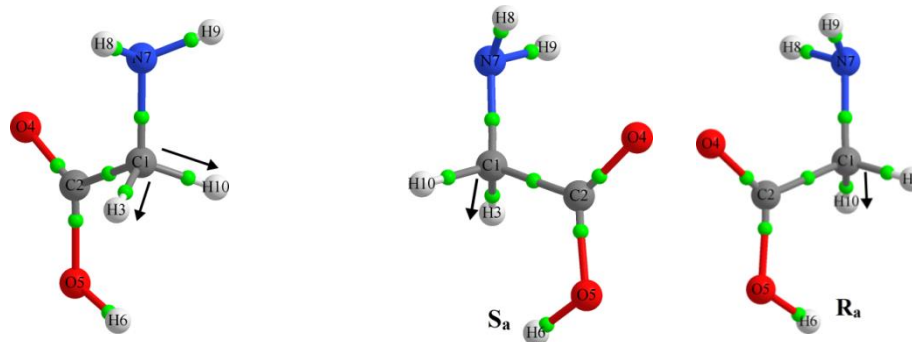
Scheme 1. The molecular graphs of glycine (left panel) with arrows indicating the directions of the positive electric (+)**E**-field of the C1-H3 *BCP* bond-path and C1-H10 *BCP* bond-path. The unlabeled green spheres indicate the bond critical points (*BCPs*). The S_a and R_a stereoisomers (right panel) are defined for alignment of the (+)**E**-field along each of the C1-H3 *BCP* bond-path and C1-H10 *BCP* bond-path respectively.

E-fields are known to alter a PES in general[40]–[46]. In extraterrestrial regions, several molecular and ionic species in excited states generated by a strong electric field which can polarize chirality have been observed[47]. Recently, some of the current authors applied a directional (±)**E**-field on the ethene molecule and demonstrated atomic polarization of the shifted C-C and C-H bond critical points (*BCPs*)[48] . The recent Perspective by Shaik *et al.* considers the prospects of oriented external-electric-fields (OEEF), and other electric-field types, as 'smart reagents', for the control of reactivity and structure for chemical catalysis[49].

We will investigate the applicability of the stress tensor trajectory $\mathbb{T}_\sigma(s)$ formalism as a molecular similarity measure by determination of any proportionate response to the application of an **E**-field to formally achiral glycine. The creation of enantiomers using formally achiral glycine enables the use of lower **E**-fields, resulting in less structural distortion, to manipulate the S and R chirality than would be the case with chiral compounds. We will use a wide range of **E**-fields from $\pm 20 \times 10^{-4}$ a.u. to $\pm 200 \times 10^{-4}$ a.u., $\approx \pm 1.1 \times 10^9$ Vm^{-1} to 11×10^9 Vm^{-1}, which includes **E**-fields that are easily accessible experimentally, for example within a Scanning Tunneling Microscope (STM).

2. Theoretical Background and Computational Details

Construction of stress tensor trajectory $\mathbb{T}_\sigma(s)$ of the torsional bond critical point

The background of QTAIM and next generation QTAIM (NG-QTAIM)[34], [50]–[55] with explanations is provided in the **Supplementary Materials S1**, along with the procedure to generate the stress tensor trajectories $\mathbb{T}_\sigma(s)$. In this investigation we will use Bader's formulation of the stress tensor[32] within the QTAIM partitioning, which is a standard option in the QTAIM AIMAll[56] suite. The ellipticity, ε, quantifies the relative accumulation of the electronic charge density $\rho(\mathbf{r_b})$ distribution in the two directions perpendicular to the bond-path at a Bond Critical Point (*BCP*) with position $\mathbf{r_b}$. For values of the ellipticity $\varepsilon > 0$, the shortest and longest axes of the elliptical distribution of $\rho(\mathbf{r_b})$ are associated with the λ_1 and λ_2 eigenvalues, respectively, and the ellipticity is defined as $\varepsilon = |\lambda_1|/|\lambda_2| - 1$. We earlier demonstrated that the most preferred direction for bond displacement, corresponding to most preferred direction of electronic charge density displacement, is the $\mathbf{e_{1\sigma}}$ eigenvector of the stress tensor[48]. Previously, we established the stress tensor trajectory $\mathbb{T}_\sigma(s)$ classifications of S and R based on the counterclockwise (CCW) vs. clockwise (CW) torsions for the $\underline{\mathbf{e}}_{1\sigma}.\mathbf{dr}$ components of $\mathbb{T}_\sigma(s)$ for lactic acid and alanine[30]. The calculation of the stress tensor trajectory $\mathbb{T}_\sigma(s)$ for the torsional *BCP* is undertaken using the frame of reference defined by the mutually perpendicular stress tensor eigenvectors $\{\pm\underline{\mathbf{e}}_{1\sigma},\pm\underline{\mathbf{e}}_{2\sigma},\pm\underline{\mathbf{e}}_{3\sigma}\}$ at the torsional *BCP*, corresponding to the *minimum energy geometry*. This frame is referred to as the stress tensor trajectory space (also referred to as $\mathbb{U}_\sigma$-space). This frame of reference is also used to construct *all* subsequent points along the $\mathbb{T}_\sigma(s)$ for dihedral torsion angles in the range -180.0º $\leq \theta \leq$ +180.0º, where $\theta = 0.0$º corresponds to the minimum energy geometry. We adopt the convention that CW circular rotations correspond to the range -180.0° $\leq \theta \leq$ 0.0° and CCW circular rotations to the range 0.0° $\leq \theta \leq$ +180.0°. To be consistent with optical experiments, we defined from the $\mathbb{T}_\sigma(s)$ that S (left-handed) character is dominant over R character (right-handed) for values of (CCW) > (CW) components of the $\mathbb{T}_\sigma(s)$. The $\mathbb{T}_\sigma(s)$ is constructed using the change in position of the *BCP*, referred to as $\mathbf{dr}$, for all displacement steps $\mathbf{dr}$ of the calculation. Each <u>finite</u> *BCP* shift vector $\mathbf{dr}$ is mapped to a point $\{(\underline{\mathbf{e}}_{1\sigma}\cdot\mathbf{dr}), (\underline{\mathbf{e}}_{2\sigma}\cdot\mathbf{dr}), (\underline{\mathbf{e}}_{3\sigma}\cdot\mathbf{dr})\}$ in sequence, forming the $\mathbb{T}_\sigma(s)$, constructed from the vector dot products (the dot product is a projection, or a measure of vectors being parallel to each other) of the stress tensor $\mathbb{T}_\sigma(s)$ eigenvector components evaluated at the *BCP*. The projections of $\mathbf{dr}$ are respectively associated with the bond torsion: $\underline{\mathbf{e}}_{1\sigma}.\mathbf{dr} \rightarrow$ bond-twist, $\underline{\mathbf{e}}_{2\sigma}.\mathbf{dr} \rightarrow$ bond-flexing and $\underline{\mathbf{e}}_{3\sigma}.\mathbf{dr} \rightarrow$ bond-anharmonicity[30], [53]–[55], [57]–[59].

The chirality $\mathbb{C}_\sigma$ is defined by the difference in the maximum projections (the dot product of the stress tensor $\mathbf{e_{1\sigma}}$ eigenvector and the *BCP* shift $\mathbf{dr}$) of the $\mathbb{T}_\sigma(s)$ values between the CCW and CW torsions $\mathbb{C}_\sigma =$ $[(\mathbf{e_{1\sigma}}\cdot\mathbf{dr})_{max}]_{CCW}$ - $[(\mathbf{e_{1\sigma}}\cdot\mathbf{dr})_{max}]_{CW}$. These torsions correspond to the CW (-180.0° $\leq \theta \leq$ 0.0°) and CCW (0°

$\leq \theta \leq 180.0°$) directions of the torsion θ. The chirality $\mathbb{C}_\sigma$ quantifies the bond torsion direction CCW vs. CW, i.e. *circular* displacement, since $\mathbf{e}_{1\sigma}$ is the most preferred direction of charge density accumulation. The least preferred displacement of a *BCP* in the $\mathbb{U}_\sigma$-space distortion set $\{\mathbb{C}_\sigma, \mathbb{F}_\sigma, \mathbb{A}_\sigma\}$ is the bond-flexing $\mathbb{F}_\sigma$, defined as $\mathbb{F}_\sigma = [(\mathbf{e}_{2\sigma} \cdot \mathbf{dr})_{\mathbf{max}}]_{\mathbf{CCW}} - [(\mathbf{e}_{2\sigma} \cdot \mathbf{dr})_{\mathbf{max}}]_{\mathbf{CW}}$. The bond-flexing $\mathbb{F}_\sigma$ therefore provides a measure of the 'flexing-strain' that a bond-path is under when, for instance, subjected to an external force such as an **E**-field. The chiral asymmetry that we refer to as the bond-anharmonicity $\mathbb{A}_\sigma$, defined as $\mathbb{A}_\sigma = [(\mathbf{e}_{3\sigma} \cdot \mathbf{dr})_{\mathbf{max}}]_{\mathbf{CCW}} - [(\mathbf{e}_{3\sigma} \cdot \mathbf{dr})_{\mathbf{max}}]_{\mathbf{CW}}$ quantifies the direction of *axial* displacement of the bond critical point (*BCP*) in response to the bond torsion (CCW vs. CW), i.e. the sliding of the *BCP* along the bond-path[59]. The sign of the chirality determines the dominance of $\mathbf{S}_\sigma$ ($\mathbb{C}_\sigma > 0$) and $\mathbf{R}_\sigma$ ($\mathbb{C}_\sigma < 0$) character, see **Tables 2-3**. The bond-anharmonicity $\mathbb{A}_\sigma$ determines the dominance of $\mathbf{S}_\sigma$ or $\mathbf{R}_\sigma$ character with respect to the *BCP* sliding along the bond-path as a consequence of the bond-torsion. $\mathbb{A}_\sigma > 0$ indicates dominant $\mathbf{S}_\sigma$ character and the converse is true for $\mathbb{A}_\sigma < 0$. The reason for calculating the $\mathbb{T}_\sigma(s)$ by varying the torsion θ is to detect values of the bond-anharmonicity $\mathbb{A}_\sigma \neq 0$, i.e. *BCP* sliding.

The stereoisomeric excess $\mathbb{X}_\sigma$ is defined as the ratio of the chirality $\mathbb{C}_\sigma$ values of S and R stereoisomers and therefore a value of $\mathbb{X}_\sigma > 1$ demonstrates a preference for the $\mathbf{S}_\sigma$ over the $\mathbf{R}_\sigma$ stereoisomer. The **E**-field amplification $\mathbb{EA}_\sigma$, is defined as the ratio $\mathbb{EA}_\sigma = \mathbb{C}_\sigma / \mathbb{C}_\sigma|_{\mathbf{E}=0}$, e.g. as a consequence of the changes that occur in an **E**-field.

Computational Details

An iterative process is employed to create the two isomers in the presence of an electric field. To create the S_a and R_a stereoisomers, a directed **E**-field is applied parallel (+**E**) or anti-parallel (-**E**) to each of the C1-H3 or C1-H10 *BCP* bond-paths (see **Scheme 1** for atom labeling). We assign the label S_a in cases where the C1-H3 *BCP* bond-path length > C1-H10 *BCP* bond-path length and the label R_a if the C1-H10 *BCP* bond-path length > C1-H3 *BCP* bond-path length. Each stereoisomer is subjected to a two-step iterative process consisting of (i) a molecule alignment step in which the alpha C1 atom is fixed at the origin of the coordinate frame: the selected C-H is aligned along a reference axis with the positive sense of the axis from C to H and the N atom consistently aligned in the same plane. This is followed by (ii) a constrained optimization step with the selected electric field applied along the reference axis: the default G09 sign convention for the field relative to the reference axis is used. This two-step process is repeated ten times, ensuring the consistency of the field application direction and the chosen bond (C1-H3 or C1-H10) direction. The resulting structures are then used in the subsequent torsion calculations, with the C1-H3 and C1-H10 bond lengths constrained to their field-optimized values.

The achiral glycine is subjected to **E**-fields = $\pm 20 \times 10^{-4}$ a.u., $\pm 100 \times 10^{-4}$ a.u. and $\pm 200 \times 10^{-4}$ a.u. before the resultant structure is twisted to construct the trajectories $\mathbb{T}_\sigma(s)$ from the series of rotational isomers -180.0°

$\leq \theta \leq +180.0°$ for the torsional *BCPs* (the C1-N7 *BCP* and the C1-C2 *BCP)* of glycine. Note that these dihedral angle definitions traverse the C-C bond in opposite directions, i.e. C2→C1 and C1→C2; therefore the definitions of CCW and CW are inverted for the C1-N7 torsion and the C1-C2 torsion. We determine the direction of torsion as CCW or CW from an increase or a decrease in the dihedral angle, respectively.

Single-point calculations were then performed on each scan geometry, converged to $< 10^{-10}$ RMS change in the density matrix and $< 10^{-8}$ maximum change in the density matrix to yield the final wavefunctions for analysis. QTAIM and stress tensor analysis was performed with the AIMAll[56] suite on each wave function obtained in the previous step. All molecular graphs were additionally confirmed to be free of non-nuclear attractor critical points.

3. Results and discussions

The $\mathbb{U}_\sigma$-space distortion set {$\mathbb{C}_\sigma$, $\mathbb{F}_\sigma$, $\mathbb{A}_\sigma$} for formally achiral and chiral molecules

The insufficiency of scalar measures for determining chirality or chiral asymmetry is provided in the **Supplementary Materials S2.** The construction of the stress tensor trajectories $\mathbb{T}_\sigma(s)$, however, involves the required additional symmetry breaking in the form of the $\underline{e}_{3\sigma}$ eigenvector, making it possible to distinguish the CCW and CW preferences for the torsional C1-C2 *BCP*. The presence of non-overlapping $\mathbb{T}_\sigma(s)$ for the CCW and CW torsions for both the C1-N7 *BCP* and the C1-C2 *BCP* demonstrates the uniqueness of the $\mathbb{T}_\sigma(s)$ of the CCW and CW torsions.

The CCW and CW stress tensor trajectories $\mathbb{T}_\sigma(s)$ of the C1-N7 *BCP* show significant differences by visual inspection, where the form of the CCW $\mathbb{T}_\sigma(s)$ indicates a more helical morphology than is the case for the CW $\mathbb{T}_\sigma(s)$. In contrast, the CCW and CW $\mathbb{T}_\sigma(s)$ of the C1-C2 *BCP* appear, by visual inspection, to display near mirror symmetry between the CCW and CW components. It can also be seen, on the same scale, that the $\mathbb{T}_\sigma(s)$ of the (dominant) torsional C1-N7 *BCP* is larger than that of the torsional C1-C2 *BCP*.
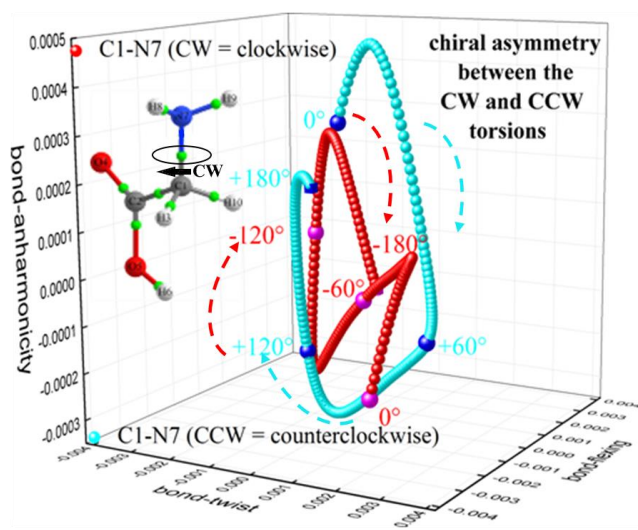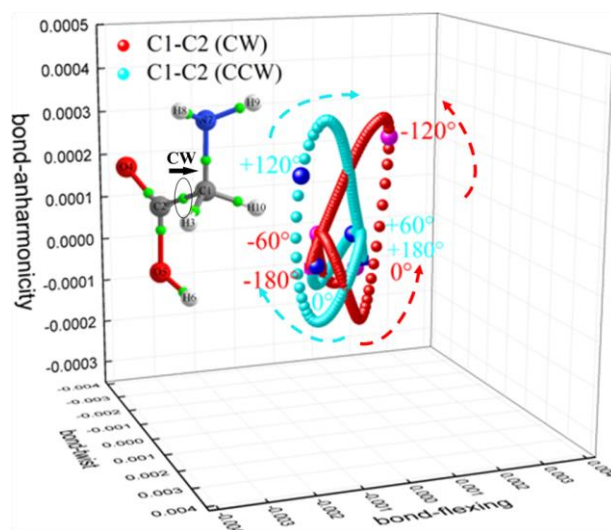
(a)   **(b)**

Figure 1. The $\mathbb{T}_\sigma(s)$ of the CW (-180.0° $\leq \theta \leq$ 0.0°) and CCW (0° $\leq \theta \leq$ 180.0°) rotations of the torsional C1-N7 *BCP* and C1-C2 *BCP* of glycine with the CW directions of torsion indicated, are presented in sub-figures **(a)** and **(b)** respectively. The $\mathbb{T}_\sigma(s)$ axes possess mappings $\underline{e}_{1\sigma}.\mathbf{dr} \rightarrow$ bond-twist, $\underline{e}_{2\sigma}.\mathbf{dr} \rightarrow$ bond-flexing, $\underline{e}_{3\sigma}.\mathbf{dr} \rightarrow$ bond-anharmonicity, where **dr** is a finite *BCP* shift vector, see the **Theoretical Background and Computational Details** section and **Table 1**. Molecular graphs are inset in their respective sub-panels: unlabeled green spheres represent bond critical points (*BCP*s).

In our previous work[30] we established the stress tensor trajectory $\mathbb{T}_\sigma(s)$ classifications of S and R based on the CCW vs. CW torsions for the $\underline{e}_{1\sigma}.\mathbf{dr}$ components of $\mathbb{T}_\sigma(s)$ for lactic acid and alanine where distinct helical shaped $\mathbb{T}_\sigma(s)$ are present. The chirality $\mathbb{C}_\sigma$ is defined in terms of the most preferred component, $\underline{e}_{1\sigma}.\mathbf{dr} \rightarrow$ bond-twist. Values of the chirality $\mathbb{C}_\sigma > 0$ for the CCW > CW torsion demonstrate a preference for $\mathbf{S}_\sigma$ compared to $\mathbf{R}_\sigma$, see the **Theoretical Background and Computational Details** section. The $\mathbb{T}_\sigma(s)$ for the entries of **Tables 1-3** as well as those of the C1-H3/C1-H10 *BCP*s are provided in the **Supplementary Materials S3-S5**. The corresponding $\mathbb{T}_\sigma(s)$ for connectivity $n = 4$, number of distinct chemical groups $m = 3$, i.e. formally achiral glycine, possesses loop-like topologies but lacks the distinct helical forms of the chiral molecules lactic acid and alanine, which have $n = 4$ and $m = 4$.

Table 1(a). The maximum stress tensor projections {bond-twist $_{max}$, bond-flexing $_{max}$, bond-anharmonicity$_{max}$}, for the S and R stereoisomers for the torsional C1-C2 *BCP* of chiral lactic acid and alanine are presented; all entries have been multiplied by 10^3, also see the caption of **Figure 1.** The connectivity n of the fixed reference C1 atom is indicated.

{bond-twist$_{max}$, bond-flexing$_{max}$, bond-anharmonicity$_{max}$}

	S_a		R_a	
	CW	**CCW**	**CW**	**CCW**
Molecule				
n = 4				
Lactic acid	{1.8998,0.9708,0.8803}	{1.9782,1.0769,0.8835}	{1.9763,1.0657,0.8843}	{1.8989, 0.9668, 0.8814}
Alanine	{2.1108,0.4132,0.8454}	{2.2257,0.4443,0.8439}	{2.2278,0.4439,0.8435}	{2.1092, 0.4135, 0.8458}

Table 1(b). The values of the chirality $\mathbb{C}_\sigma = [(e_{1\sigma} \cdot dr)_{max}]_{CCW} - [(e_{1\sigma} \cdot dr)_{max}]_{CW}$, bond-flexing $\mathbb{F}_\sigma = [(e_{2\sigma} \cdot dr)_{max}]_{CCW} - [(e_{2\sigma} \cdot dr)_{max}]_{CW}$ and bond-anharmonicity $\mathbb{A}_\sigma = [(e_{3\sigma} \cdot dr)_{max}]_{CCW} - [(e_{3\sigma} \cdot dr)_{max}]_{CW}$ of the torsional C1-N7 *BCP* for the isotopomers of glycine are presented, also see **Table 1(a)**, all entries are multiplied by 10^3. The stereoisomeric excess $\mathbb{X}_\sigma$ is defined as the ratio of the magnitude of the $\mathbb{C}_\sigma$ values of the S and R stereoisomers of the torsional C1-N7 *BCP*.

	S	R	
Molecule	$\{\mathbb{C}_\sigma, \mathbb{F}_\sigma, \mathbb{A}_\sigma\}$	$\{\mathbb{C}_\sigma, \mathbb{F}_\sigma, \mathbb{A}_\sigma\}$	$\mathbb{X}_\sigma$
n = 4			
Lactic acid	{0.0783[$\mathbf{S_\sigma}$], 0.1061[$\mathbf{S_\sigma}$], 0.0032[$\mathbf{S_\sigma}$]}	{-0.0773[$\mathbf{R_\sigma}$], -0.0989[$\mathbf{R_\sigma}$], -0.0029[$\mathbf{R_\sigma}$]}	1.1363
Alanine	{0.1149[$\mathbf{S_\sigma}$], 0.0311[$\mathbf{S_\sigma}$], -0.0015[$\mathbf{R_\sigma}$]}	{-0.1186[$\mathbf{R_\sigma}$], -0.0304[$\mathbf{R_\sigma}$], 0.0023[$\mathbf{S_\sigma}$]}	0.6296

For lactic acid and alanine the presence of S and R stereoisomers means that we can also consider the magnitude of the stereoisomeric excess $\mathbb{X}_\sigma$. We find for lactic acid a preference for the S stereoisomer since $\mathbb{X}_\sigma > 1$ (= 1.1363), corresponding to values of the chirality $\mathbb{C}_\sigma = 0.0783$ and $\mathbb{C}_\sigma = -0.0773$ for the S and R stereoisomers respectively. For alanine the chirality $\mathbb{C}_\sigma$ is much larger than the bond-flexing $\mathbb{F}_\sigma$ contribution for both alanine S and R stereoisomers; the converse is true for lactic acid.

A strong preference for the R stereoisomer is found for alanine due to the presence of the larger magnitude of $\mathbb{C}_\sigma = -0.1186$ (compared with $\mathbb{C}_\sigma = 0.1149$ for the S stereoisomer) and $\mathbb{X}_\sigma < 1$ (= 0.6296), see **Table 1(b)**.

Table 2(a). For the formally achiral glycine molecule in the absence of an electric (**E**)-field, the maximum stress tensor projections {bond-twist$_{max}$, bond-flexing$_{max}$, bond-anharmonicity$_{max}$} for the torsional C1-N7 *BCP* and torsional C1-C2 *BCP*, where **dr** is a finite *BCP* shift vector, see the caption of **Figure 1** for further details. The connectivity n of the fixed reference C1 atom is indicated.

	{bond-twist$_{max}$, bond-flexing$_{max}$, bond-anharmonicity$_{max}$}	
	CW	**CCW**
Molecule		
n = 4		
glycine (C1-N7)	{3.26019, 1.60696, 0.54036}	{3.44982, 1.27642, 0.71997}
glycine (C1-C2)	{1.84486, 1.60472, 0.46961}	{1.90176, 1.59342, 0.47094}

Table 2(b). Formally achiral glycine in the absence of an electric (**E**)-field, the values of the chirality $\mathbb{C}_\sigma$, bond-flexing $\mathbb{F}_\sigma$ and bond-anharmonicity $\mathbb{A}_\sigma$, also see **Table 1(a)**.

Molecule	$\{\mathbb{C}_\sigma, \mathbb{F}_\sigma, \mathbb{A}_\sigma\}$
n = 4	
glycine (C1-N7)	{0.18963[**S$_\sigma$**], -0.33054[**R$_\sigma$**], 0.17961[**S$_\sigma$**]}
glycine (C1-C2)	{0.05690[**S$_\sigma$**], -0.01130[**R$_\sigma$**], 0.00133[**S$_\sigma$**]}

We now present the quantification of the chirality $\mathbb{C}_\sigma$, which is defined in terms of the most preferred component, $\underline{e}_{1\sigma}.dr \rightarrow$ bond-twist, for the CCW and CW torsions. The presence of a positive value for the glycine chirality $\mathbb{C}_\sigma$ demonstrates that **S$_\sigma$** character dominates over **R$_\sigma$** character for the $\mathbb{T}_\sigma(s)$ of the dominant torsional C1-N7 *BCP*, see **Table 1(a)**. This is because the CCW torsion occurs more readily, which is apparent from the $\underline{e}_{1\sigma}.dr$ component being 5.51% larger than that of the CW torsion, see **Table 1(a)**. The corresponding value of the chirality $\mathbb{C}_\sigma$ for the torsional C1-C2 *BCP* also demonstrates **S$_\sigma$** character, where the CCW $\underline{e}_{1\sigma}.dr$ component is 3.16 % larger than the CW $\underline{e}_{1\sigma}.dr$ component, see **Table 1(b)**. For the glycine torsional C1-C2 *BCP* the chirality $\mathbb{C}_\sigma = 0.057$, bond-flexing $\mathbb{F}_\sigma = -0.011$ and the bond-anharmonicity $\mathbb{A}_\sigma = 0.0013$, see **Table 2(b)**. Although these values are small compared to the $\mathbb{C}_\sigma$, $\mathbb{F}_\sigma$ and $\mathbb{A}_\sigma$ values of the stronger torsional bond, i.e. the torsional C1-N7 *BCP*, they are more comparable to $\mathbb{C}_\sigma = 0.078$ and $\mathbb{A}_\sigma = 0.003$ of the torsional C1-C2 *BCP* of the S-stereoisomer of lactic acid and $\mathbb{F}_\sigma = -0.030$ of the R-stereoisomer of alanine, compare **Table 1(b)** with **Table 2(b)**. For lactic acid the S-stereoisomer possesses a larger value of $\mathbb{C}_\sigma$ than the R-stereoisomer, consistent with earlier work[30], see **Table 2(b)**. The corresponding $\mathbb{C}_\sigma$ results for the alanine torsional C1-C2 *BCP* indicate a preference for the R-stereoisomer, in keeping with experiment[60].
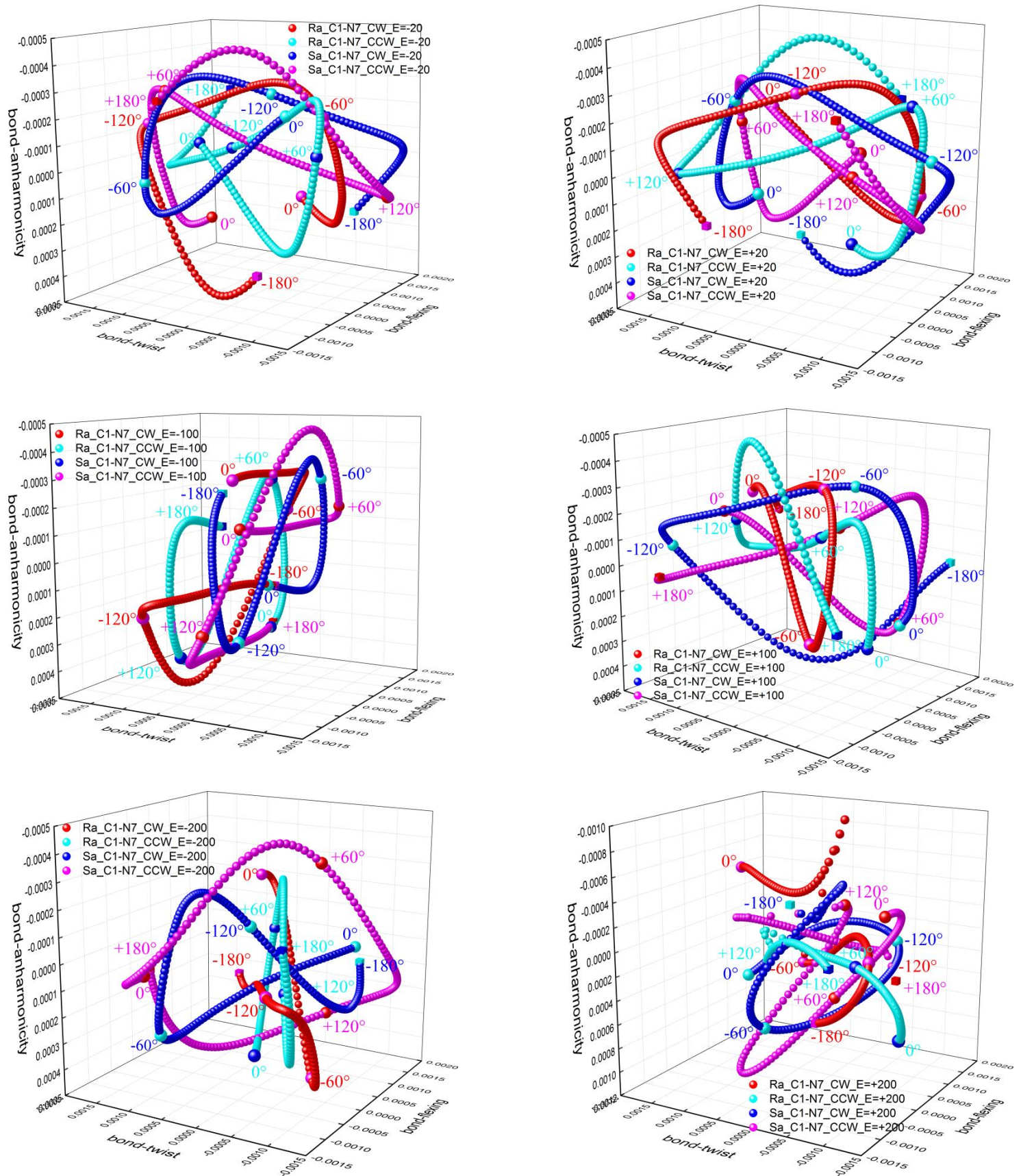
Figure 2. The $\mathbb{T}_\sigma(s)$ of the CW ($\theta = 0.0°$, $-60.0°$, $-120.0°$, $-180.0°$) and CCW ($\theta = 0.0°$, $60.0°$, $120.0°$, $180.0°$) of the torsional C1-N7 *BCP* bond-path for the **E**-fields = -20×10^{-4} au, -100×10^{-4} au and -200×10^{-4} au are presented in the left panels respectively, the corresponding **E**-fields = $+20 \times 10^{-4}$ au, $+100 \times 10^{-4}$ au and $+200 \times 10^{-4}$ au are presented in the right panels of sub-figure **(a-c)** respectively. Note, for ease of comparison of the effect of different values of the **E**-field the same axes scales are used throughout.

The $\mathbb{U}_\sigma$-space distortion set $\{\mathbb{C}_\sigma, \mathbb{F}_\sigma, \mathbb{A}_\sigma\}$ as a molecular similarity measure

We created S_a and R_a stereoisomers of glycine by applying an electric (**E**)-field to induce symmetry-breaking changes to the length of the C-H bonds attached to the alpha carbon (C1) atom, see **Table 3(a-b)** and **Figure 2**. We found that reversal of the **E**-field caused a reversal of the chirality $\mathbb{C}_\sigma$ of the S_a stereoisomer from $\mathbf{S_\sigma}$ to $\mathbf{R_\sigma}$, except for the high **E**-field $= +200\times10^{-4}$ a.u., which distorted the structure to the extent of inducing an intramolecular hydrogen bond. The corresponding reversal of the chirality $\mathbb{C}_\sigma$ also occurred for the R_a stereoisomer. The **E**-field amplification $\mathbb{E}\mathbb{A}_\sigma$ is found to increase with the application of a non-structurally distorting **E**-field, demonstrating that control of the chirality $\mathbb{C}_\sigma$ of glycine is possible in the case of negligible structural distortion.

The largest magnitudes of bond-flexing $\mathbb{F}_\sigma$ occur for both the S_a and R_a stereoisomers at $\mathbf{E} = -100\times10^{-4}$ a.u. ($\mathbb{F}_\sigma \approx 1.0$) and are approximately three times greater than for the absence of the **E**-field ($\mathbb{F}_\sigma \approx 0.33$), see **Table 2(b)**. The lowest magnitudes of the bond-flexing $\mathbb{F}_\sigma$ occur at $\mathbf{E} = +100\times10^{-4}$ a.u. ($\mathbb{F}_\sigma \approx 0.1$) for both the S_a and R_a stereoisomers and are approximately a third of those in the absence of the **E**-field ($\mathbb{F}_\sigma \approx 0.33$). This indicates that at $\mathbf{E} = -100\times10^{-4}$ a.u. and $\mathbf{E} = +100\times10^{-4}$ a.u., the S_a and R_a stereoisomers experience the least and greatest degree of torsional C1-N7 *BCP* bond-strain, respectively.

Table 3(a). The maximum stress tensor projections {bond-twist $_{max}$, bond-flexing $_{max}$, bond-anharmonicity$_{max}$}, of the dominant torsional C1-N7 *BCP* for the electric field induced S_a and R_a stereoisomers of glycine are presented; all entries have been multiplied by 10^3, also see the caption of **Table 1(a).**

	{bond-twist$_{max}$, bond-flexing$_{max}$, bond-anharmonicity$_{max}$}			
	S_a		R_a	
	CW	CCW	CW	CCW
Molecule				
($\pm$) electric-field$\times10^{-4}$ a.u				
-20	{3.1999, 1.3789, 0.5157}	{3.4961, 1.0657, 0.7231}	{3.4229, 1.1970, 0.7757}	{3.2624, 1.5383, 0.5502}
-100	{0.3698, 2.9198, 0.6052}	{0.7745, 3.9570, 0.7739}	{0.7527, 3.9581, 0.7784}	{0.3735, 2.9209, 0.6039}
-200	{1.5422, 2.8812, 0.5281}	{2.2128, 3.4541, 0.7779}	{2.2930, 3.4013, 0.6959}	{1.5461, 2.5344, 0.5428}
+20	{3.4216, 1.1451, 0.7773}	{3.2804, 1.4972, 0.5525}	{3.2203, 1.3400, 0.5365}	{3.5034, 1.0231, 0.7204}
+100	{3.1570, 2.2760, 0.7501}	{2.6790, 2.3690, 0.5560}	{2.6209, 2.2755, 0.5359}	{3.3027, 2.2004, 0.6971}
+200	{1.6560, 1.5748, 1.2344}	{1.9578, 1.2426, 1.4150}	{2.6512, 1.5395, 1.7706}	{3.0119, 1.8427, 0.5820}

Table 3(b). The chirality $\mathbb{C}_\sigma$, bond-flexing $\mathbb{F}_\sigma$ and bond-anharmonicity $\mathbb{A}_\sigma$ and the **E**-field amplification $\mathbb{EA}_\sigma$ of the dominant torsional C1-N7 *BCP* for the electric field induced S_a and R_a stereoisomers of glycine. The **E**-field amplification $\mathbb{EA}_\sigma$, is defined for each S_a and R_a stereoisomer as the ratio $\mathbb{EA}_\sigma = \mathbb{C}_\sigma/\mathbb{C}_\sigma|_{E=0}$, see also **Table 3(a)**. For comparison the results corresponding to **E**-field = 0 see **Table 1(b)**.

Molecule	S_a $\{\mathbb{C}_\sigma, \mathbb{F}_\sigma, \mathbb{A}_\sigma\}$	$\mathbb{EA}_\sigma$	R_a $\{\mathbb{C}_\sigma, \mathbb{F}_\sigma, \mathbb{A}_\sigma\}$	$\mathbb{EA}_\sigma$	$\mathbb{X}_\sigma$
$(\pm)$ electric-field$\times10^{-4}$ a.u					
-20	$\{0.296[\mathbf{S_\sigma}], -0.313[\mathbf{R_\sigma}], 0.207[\mathbf{S_\sigma}]\}$	1.558	$\{-0.161[\mathbf{R_\sigma}], 0.341[\mathbf{S_\sigma}], -0.226[\mathbf{R_\sigma}]\}$	-0.847	1.839
-100	$\{0.404[\mathbf{S_\sigma}], 1.037[\mathbf{S_\sigma}], 0.169[\mathbf{S_\sigma}]\}$	2.126	$\{-0.381[\mathbf{R_\sigma}], -1.037[\mathbf{R_\sigma}], -0.174[\mathbf{R_\sigma}]\}$	-2.005	1.060
-200	$\{0.751[\mathbf{S_\sigma}], 0.573[\mathbf{S_\sigma}], 0.168[\mathbf{S_\sigma}]\}$	3.953	$\{-0.667[\mathbf{R_\sigma}], -0.867[\mathbf{R_\sigma}], -0.235[\mathbf{R_\sigma}]\}$	-3.512	1.126
+20	$\{-0.142[\mathbf{R_\sigma}], 0.352[\mathbf{S_\sigma}], -0.225[\mathbf{R_\sigma}]\}$	-0.747	$\{ 0.283[\mathbf{S_\sigma}], -0.317[\mathbf{R_\sigma}], 0.183[\mathbf{S_\sigma}]\}$	1.489	0.502
+100	$\{-0.478[\mathbf{R_\sigma}], 0.093[\mathbf{S_\sigma}], -0.194[\mathbf{R_\sigma}]\}$	2.516	$\{ 0.681[\mathbf{S_\sigma}], -0.075[\mathbf{R_\sigma}], 0.161[\mathbf{S_\sigma}]\}$	3.584	0.702
+200	$\{ 0.302[\mathbf{S_\sigma}], -0.332[\mathbf{R_\sigma}], 0.181[\mathbf{S_\sigma}]\}$	1.589	$\{ 0.361[\mathbf{R_\sigma}], 0.303[\mathbf{S_\sigma}], -1.189[\mathbf{R_\sigma}]\}$	1.900	0.837

Conclusions

We have demonstrated that formally achiral glycine can be made chiral by the application of an electric (**E**)-field that induces the formation of S_a and R_a stereoisomers. We furthermore demonstrated that the chirality $\mathbb{C}_\sigma$ can be controlled. Calculating the chirality in the form of the chiral discrimination $\mathbb{C}_\sigma$ also enables the determination of the bond-flexing $\mathbb{F}_\sigma$ and bond-anharmonicity $\mathbb{A}_\sigma$ for both formally achiral and chiral molecules. This investigation establishes and quantifies the robustness of the **E**-field-induced chirality $\mathbb{C}_\sigma$ of stereoisomers of glycine (S_a or R_a). We demonstrate that chirality increases with increase in the **E**-field, as indicated by the increase in the **E**-field amplification $\mathbb{EA}_\sigma$ with the application of a non-structurally distorting **E**-field. The bond-anharmonicity $\mathbb{A}_\sigma$ was found to be rather invariant to the magnitude of the applied **E**-field, as was the stereoisomeric excess $\mathbb{X}_\sigma$. The magnitude of the bond-flexing $\mathbb{F}_\sigma$, however, showed significant variations, both larger and smaller than in the absence of an applied **E**-field, with noticeable increases and decreases for $\mathbf{E} = -100\times10^{-4}$ a.u. and $\mathbf{E} = +100\times10^{-4}$ a.u., respectively. This finding indicates the role of monitoring the **E**-field direction to minimize the bond-strain, i.e. the magnitude of the bond-flexing $\mathbb{F}_\sigma$, to achieve less destructive manipulation of the chirality $\mathbb{C}_\sigma$.

The proportional response of the chirality $\mathbb{C}_\sigma$, **E**-field amplification $\mathbb{EA}_\sigma$ and the stereoisomeric excess, $\mathbb{X}_\sigma$ for modest **E**-field demonstrates their potential use as a molecular similarity measure. The ability to track and control chirality and associated properties could be used in asymmetric autocatalysis[61] or contribute to the design of enantioselective catalytic processes[62]. Another potential application would be in heterogeneous enantioselective catalysis. This is normally achieved through adsorbing chiral molecules on a surface. Using molecules that are chiral only in the presence of an **E**-field allows the use of a much wider range of molecules and allows changing the chirality of the product by changing the direction of the **E**-field. Besides catalysis, **E**-field or laser-field induced chirality could be used to grow chiral MOFs (metal organic

frameworks) or other self-assembled structures on a surface.

Future avenues of investigation could also follow on from the recent work of Ayuso *et al.,* generating synthetic controllable chiral light for ultrafast imaging of chiral dynamics in gases, liquids and solids[63]. This can also be used to imprint chirality on achiral matter efficiently[64] and may lead to insights into laser-driven achiral–chiral phase transitions in matter[65]. Our approach could be a powerful analytical method to open up a wide scientific field for chiral solid state and molecular systems to track and quantify the chirality for the first time, e.g. in a wide range of molecular devices including substituted dithienylethene photochromic switches[66], azobenzene chiroptical switches[67] and the design of chiral-optical molecular rotary motors[68].

Funding Information

References

[1] V. Prelog, *Croat. Chem. Acta*, **2006**, *79*, 49-57 (XLIX-LVII).

[2] L. Pasteur, *Ann Chim Phys*, **1850**, *28*, 56–99.

[3] N. Katsonis, F. Lancia, D. A. Leigh, L. Pirvu, A. Ryabchun, F. Schaufelberger, *Nat. Chem.*, **2020**, DOI:10.1038/s41557-020-0517-1.

[4] S. M. Morrow, A. J. Bissette, S. P. Fletcher, *Nat. Nanotechnol.*, **2017**, DOI:10.1038/nnano.2017.62.

[5] J. E. Hein, D. G. Blackmond, *Acc. Chem. Res.*, **2012**, DOI:10.1021/ar200316n.

[6] J. L. Bada, *Nature*, **1995**, DOI:10.1038/374594a0.

[7] R. Breslow, Z.-L. Cheng, *Proc. Natl. Acad. Sci.*, **2009**, DOI:10.1073/pnas.0904350106.

[8] G. Pályi, C. Zucchi, L. Caglioti, Eds., in Progress in Biochirality; Elsevier Science, ISBN 978-0-08-044396-6, **2004**; 1st ed.

[9] Y. Chen, K. Deng, S. Lei, R. Yang, T. Li, Y. Gu, Y. Yang, X. Qiu, C. Wang, *Nat. Commun.*, **2018**, DOI:10.1038/s41467-018-05218-0.

[10] W. A. Bonner, *Orig. Life Evol. Biosph.*, **1991**, DOI:10.1007/BF01809580.

[11] R. Wallace, *C. R. Biol.*, **2011**, DOI:10.1016/j.crvi.2011.01.001.

[12] N. A. Hawbaker, D. G. Blackmond, *Nat. Chem.*, **2019**, DOI:10.1038/s41557-019-0321-y.

[13] H. Flack, *Acta Crystallogr. Sect. A*, **2009**, *65*, 371–389.

[14] M. Francl, *Nat. Chem.*, **2019**, DOI:10.1038/s41557-019-0283-0.

[15] A. F. Zahrt, S. E. Denmark, *Tetrahedron*, **2019**, DOI:10.1016/j.tet.2019.02.007.

[16] H. Zabrodsky, D. Avnir, *J. Am. Chem. Soc.*, **1995**, DOI:10.1021/ja00106a053.

[17] K. Mislow, P. Bickart, *Isr. J. Chem.*, **1976**, DOI:https://doi.org/10.1002/ijch.197600002.

[18] M. Petitjean, *Entropy*, **2003**, DOI:10.3390/e5030271.

[19] M. H. Jamróz, J. E. Rode, S. Ostrowski, P. F. J. Lipiński, J. Cz. Dobrowolski, *J. Chem. Inf. Model.*, **2012**, DOI:10.1021/ci300057h.

[20] G. M. Maggiora, V. Shanmugasundaram, Molecular Similarity Measures, *Chemoinformatics and Computational Chemical Biology*. Humana Press, Totowa, NJ, 39–100, 2011.

[21] P. Willett, Molecular Similarity Approaches in Chemoinformatics: Early History and Literature Status, *Frontiers in Molecular Design and Chemical Information Science - Herman Skolnik Award Symposium 2015: Jürgen Bajorath*, *1222*. American Chemical Society, , 67–89, 2016.

[22] S. Kearnes, V. Pande, *J. Comput. Aided Mol. Des.*, **2016**, DOI:10.1007/s10822-016-9959-3.

[23] A. Wagner, H.-J. Himmel, *J. Chem. Inf. Model.*, **2017**, DOI:10.1021/acs.jcim.6b00516.

[24] S. A. Bero, A. K. Muda, Y. H. Choo, N. A. Muda, S. F. Pratama, *J. Phys. Conf. Ser.*, **2017**, DOI:10.1088/1742-6596/892/1/012015.

[25] E. Ruch, *Acc. Chem. Res.*, **1972**, DOI:10.1021/ar50050a002.

[26] G. Moreau, *J. Chem. Inf. Comput. Sci.*, **1997**, DOI:10.1021/ci970460k.

[27] J. Aires-de-Sousa, J. Gasteiger, I. Gutman, D. Vidović, *J. Chem. Inf. Comput. Sci.*, **2004**, DOI:10.1021/ci030410h.

[28] Y. Marrero-Ponce, J. A. Castillo-Garit, E. A. Castro, F. Torrens, R. Rotondo, *J. Math. Chem.*, **2008**, DOI:10.1007/s10910-008-9386-3.

[29] D. S. Bradshaw, J. M. Leeder, M. M. Coles, D. L. Andrews, *Chem. Phys. Lett.*, **2015**, DOI:10.1016/j.cplett.2015.02.051.

[30] T. Xu, J. H. Li, R. Momen, W. J. Huang, S. R. Kirk, Y. Shigeta, S. Jenkins, *J. Am. Chem. Soc.*, **2019**, DOI:10.1021/jacs.9b00823.

[31] R. F. W. Bader, in Atoms in Molecules: A Quantum Theory; Oxford University Press, USA, New York, **1994**.

[32] R. F. W. Bader, *J. Chem. Phys.*, **1980**, DOI:10.1063/1.440457.

[33] T. Xu, S. R. Kirk, S. Jenkins, *Chem. Phys. Lett.*, **2020**, DOI:10.1016/j.cplett.2019.136907.

[34] J. H. Li, W. J. Huang, T. Xu, S. R. Kirk, S. Jenkins, *Int. J. Quantum Chem.*, **2018**,

DOI:10.1002/qua.25847.

[35] H. Nakatsuji, *J. Am. Chem. Soc.*, **1974**, DOI:10.1021/ja00808a004.

[36] R. G. A. Bone, R. F. W. Bader, *J. Phys. Chem.*, **1996**, *100*, 10892–10911.

[37] S. Jenkins, M. I. Heggie, *J. Phys. Condens. Matter*, **2000**, DOI:10.1088/0953-8984/12/49/3.

[38] P. W. Ayers, S. Jenkins, *J. Chem. Phys.*, **2009**, DOI:10.1063/1.3098140.

[39] J. L. Wolk, S. Hoz, *Can. J. Chem.*, **2014**, DOI:10.1139/cjc-2014-0354.

[40] A. Saenz, *Phys. Rev. A*, **2000**, DOI:10.1103/PhysRevA.61.051402.

[41] A. Saenz, *Phys. Rev. A*, **2002**, DOI:10.1103/PhysRevA.66.063407.

[42] Z. Medin, D. Lai, *Phys. Rev. A*, **2006**, DOI:10.1103/PhysRevA.74.062508.

[43] S. Petretti, Y. V. Vanne, A. Saenz, A. Castro, P. Decleva, *Phys. Rev. Lett.*, **2010**, DOI:10.1103/PhysRevLett.104.223001.

[44] S. Shaik, D. Mandal, R. Ramanan, *Nat. Chem.*, **2016**, DOI:10.1038/nchem.2651.

[45] S. Shaik, R. Ramanan, D. Danovich, D. Mandal, *Chem. Soc. Rev.*, **2018**, DOI:10.1039/C8CS00354H.

[46] Z. Wang, D. Danovich, R. Ramanan, S. Shaik, *J. Am. Chem. Soc.*, **2018**, DOI:10.1021/jacs.8b08233.

[47] D. Ayuso, A. Ordonez, P. Decleva, M. Ivanov, O. Smirnova, *ArXiv200405191 Phys.*, **2020**.

[48] A. Azizi, R. Momen, H. Früchtl, T. van Mourik, S. R. Kirk, S. Jenkins, *J. Comput. Chem.*, **2020**, DOI:https://doi.org/10.1002/jcc.26137.

[49] S. Shaik, D. Danovich, J. Joy, Z. Wang, T. Stuyver, *J. Am. Chem. Soc.*, **2020**, DOI:10.1021/jacs.0c05128.

[50] M. X. Hu, T. Xu, R. Momen, A. Azizi, S. R. Kirk, S. Jenkins, *Chem. Phys. Lett.*, **2017**, DOI:10.1016/j.cplett.2017.04.017.

[51] W. J. Huang, T. Xu, S. R. Kirk, M. Filatov, S. Jenkins, *Chem. Phys. Lett.*, **2018**, DOI:10.1016/j.cplett.2018.10.029.

[52] H. Guo, A. Morales-Bayuelo, T. Xu, R. Momen, L. Wang, P. Yang, S. R. Kirk, S. Jenkins, *J. Comput. Chem.*, **2016**, DOI:10.1002/jcc.24499.

[53] P. Yang, T. Xu, R. Momen, A. Azizi, S. R. Kirk, S. Jenkins, *Int. J. Quantum Chem.*, **2018**, DOI:10.1002/qua.25565.

[54] T. Xu, L. Wang, Y. Ping, T. van Mourik, H. Früchtl, S. R. Kirk, S. Jenkins, *Int. J. Quantum Chem.*, **2018**, DOI:10.1002/qua.25676.

[55] T. Xu, J. Farrell, R. Momen, A. Azizi, S. R. Kirk, S. Jenkins, D. J. Wales, *Chem. Phys. Lett.*, **2017**, DOI:10.1016/j.cplett.2016.11.028.

[56] T. A. Keith, in AIMAll, Revision 19.10.12; TK Gristmill Software, Overland Park KS, USA, **2019**.

[57] T. Xu, R. Momen, A. Azizi, T. van Mourik, H. Früchtl, S. R. Kirk, S. Jenkins, *J. Comput. Chem.*, **2019**, DOI:10.1002/jcc.25843.

[58] T. Tian, T. Xu, T. van Mourik, H. Früchtl, S. R. Kirk, S. Jenkins, *Chem. Phys. Lett.*, **2019**, DOI:10.1016/j.cplett.2019.03.013.

[59] T. Tian, T. Xu, S. R. Kirk, I. T. Rongde, Y. B. Tan, S. Manzhos, Y. Shigeta, S. Jenkins, *Phys. Chem. Chem. Phys.*, **2020**, DOI:10.1039/C9CP05879F.

[60] C. M. Stevens, P. E. Halpern, R. P. Gigger, *J. Biol. Chem.*, **1951**, *190*, 705–710.

[61] A. Matsumoto, H. Ozaki, S. Tsuchiya, T. Asahi, M. Lahav, T. Kawasaki, K. Soai, *Org. Biomol. Chem.*, **2019**, DOI:10.1039/C9OB00345B.

[62] L. C. Wilkins, R. L. Melen, *Coord. Chem. Rev.*, **2016**, DOI:10.1016/j.ccr.2016.07.011.

[63] D. Ayuso, O. Neufeld, A. F. Ordonez, P. Decleva, G. Lerner, O. Cohen, M. Ivanov, O. Smirnova, *Nat. Photonics*, **2019**, DOI:10.1038/s41566-019-0531-2.

[64] A. F. Ordonez, O. Smirnova, *Phys. Rev. A*, **2019**, DOI:10.1103/PhysRevA.99.043416.

[65] R. Cireasa, A. E. Boguslavskiy, B. Pons, M. C. H. Wong, D. Descamps, S. Petit, H. Ruf, N. Thiré, A. Ferré, J. Suarez, J. Higuet, B. E. Schmidt, A. F. Alharbi, F. Légaré, V. Blanchet, B. Fabre, S. Patchkovskii, O. Smirnova, Y. Mairesse, V. R. Bhardwaj, *Nat. Phys.*, **2015**, DOI:10.1038/nphys3369.

[66] J. J. D. de Jong, P. van Rijn, T. D. Tiemersma-Wegeman, L. N. Lucas, W. R. Browne, R. M. Kellogg, K. Uchida, J. H. van Esch, B. L. Feringa, *Tetrahedron*, **2008**, DOI:10.1016/j.tet.2008.05.129.

[67] O. Weingart, Z. Lan, A. Koslowski, W. Thiel, *J. Phys. Chem. Lett.*, **2011**, DOI:10.1021/jz200474g.

[68] A. Nikiforov, J. A. Gamez, W. Thiel, M. Filatov, *J. Phys. Chem. Lett.*, **2016**, DOI:10.1021/acs.jpclett.5b02575.